2014 23rd International Lightning Detection Conference
18 - 19 March • Tucson, Arizona, USA
5th International Lightning Meteorology Conference
20 - 21 March • Tucson, Arizona, USA

Observations of turbulent kinematics and lightning-inferred electric potential structure in a severe squall line

Eric Bruning, Vicente Salinas, Vanna Sullivan, Scott Gunter and John Schroeder
Texas Tech University
Lubbock, TX
eric.bruning@ttu.edu

***Abstract*—A severe squall line that moved across West Texas on the night of 5 June 2013 caused extensive damage, including much that was consistent with 80-90 mph winds in the vicinity of Lubbock. The storm was sampled west of Lubbock during the onset of severe winds by two Ka-band mobile radars operated by Texas Tech University (TTU), as well as the West Texas Lightning Mapping Array (WTLMA). In-situ observations by TTU StickNet probes verified the severe winds. Vertical scans with the radars were taken ahead of the storm and continuously for one hour behind the line in conditions consistent with the conceptual model for the transition zone of a mesoscale convective system. Doppler velocity observations from the radars (every 10 s at 0.33 deg beamwidth and ~10 m gate spacing) clearly resolve the turbulent kinematics, including overturning eddies in front-to-rear flow just behind the squall line. Lightning energetics are inferred from WTLMA-derived flash size and rate, allowing for a test of the idea that the turbulent structure of the convection controls the distribution of electric potential energy discharged by lightning.**

Keywords—lightning, turbulence, thunderstorm charge structure, radar

I. INTRODUCTION

Recent work by Bruning and MacGorman [2013] has examined the distribution of lightning flash sizes within thunderclouds. They noted numerous recent studies that have found relationships between the extent of flashes detected by VHF Lightning Mapping Arrays (LMAs) [Thomas et al., 2004] and storm kinematics. In particular, the smallest flashes in a storm are usually located in and near the strongest vertical velocities where turbulent eddies would be more numerous, while flashes in thunderstorm anvils and extensive stratiform clouds tend to have larger flashes. Furthermore, they note how, from basic electrostatic considerations, it can be shown that higher flash rates tend to correspond to smaller flashes, and vice versa. The purpose of this study is to further investigate the flash size distribution and its link to between turbulent kinematics by testing with high-resolution weather radar data the idea that the turbulent structure of storms and the average local flash size track one another.

Bruning and MacGorman [2013] further investigated the possibility that convective motions were the source of energy stored in the electric field between regions of potential by using a partitioned-capacitor model of charging and discharge to characterize the energy dissipated by a collection of lightning flashes. The relationship between electrical energy dissipation, flash area, and flash rate indicated by dimensional analysis was reproduced by including convective motions as the source of net electrification. They assumed that the charging current was provided by some convective velocity $w = d/T$ acting on a charge gradient in the direction parallel to d, giving

$$E_W = \frac{W_i}{\rho_a V_I} = \frac{1}{2}\frac{Q_i^2}{\rho_a \epsilon_0}\frac{d^3}{V_I^3} A_i \eta_i^2 T^2$$

where E_W is the flash energy per unit mass of air with density ρ_a, W_i is the total energy dissipated at scale size A_i, and ϵ is the permittivity of air. The total volume V_I formed by the capacitor plate separation d was divided into subvolumes V_I, which produced an ensemble of flashes occurring over time T with flash rate η. Each individually-discharging region subdivides the total area A_I into identical flash areas A_i. Each flash is responsible for a fraction Q_i of the net charge neutralized.

Bruning and MacGorman [2013] also found a predictable shape of the flash energy spectrum versus flash size $l = \sqrt{A_i}$. We now show that the total flash energy is related to the distribution of flashes at size l as follows:

$$E(l) = \frac{\rho^2 l^2 d^3}{2\epsilon_0} = Kl^2$$

$$N(l) = N_T \int_0^\infty P(l)dl$$

$$E_T = \int_0^\infty E(l)N(l)dl = KN_T \int_0^\infty l^2 P(l)dl$$

This work was supported in part by the National Science Foundation under award NSF-1063966 and NOAA's GOES-R program under NASA award NNX12AC66G. Additional support for radar operations was provided by NSF-1000160.

where N_T is the total number of flashes, and $P(l)$ is the probability density function for flash size. The total energy E_T over the collection of all flashes is the second raw moment of the flash size distribution.

Leaving aside for now the correct shape and possible skew of the flash size distribution, one may assume several different distributions (e.g., normal, gamma, lognormal) and look at the resulting formulas for total energy. For each of those distributions, it may be shown that there is a linear dependence on the product of the total flash rate and the "area" determined from the characteristic length scale of the distribution of flash sizes. There is also a dependence on the spread of the distribution.

Operational and modeling applications frequently describe lightning activity in terms of flash rate alone [e.g., Schultz et al., 2009; Barthe and Barth 2008]. This choice of formulation of parameterizations implies that, even if flash sizes vary somewhat, they do so symmetrically about a "typical" flash size, and so any underestimates due to small flashes are compensated by large ones. Therefore, skewness in the flash size distribution or variability in the average flash size with time would propose a problem for these parameterizations. One purpose of this study is to examine the differences in lightning trends when considering flash energy instead of flash rate. The simple physical model described above suggests that both the flash rate and the size statistics of those flashes matters to the total energy dissipated.

II. DATA

A. *Meteorological setting*

Data in this study are from a severe squall line that moved across West Texas on the night of 5-6 June 2013 and caused extensive damage, including much that was consistent with 80-90 mph winds in the vicinity of Lubbock. According to NWS Storm Data reports, the storm produced several severe (> 1") hail reports along with dozens of severe wind reports. The wind reports were roughly bounded by Clovis and Hobbs, NM and Abilene and San Angelo, TX, covering a large fraction of West-Central Texas. The following meteorological background provides context for our observations of the storm with high-resolution Doppler radars and the West Texas Lightning Mapping Array.

At 21 UTC on 5 June 2013, a cold front was analyzed from northeast New Mexico through Amarillo, TX and into Oklahoma. Easterly, upslope surface flow ahead of the front transported dew points in the mid-50s °F onto the caprock escarpment in West Texas. Thunderstorms had initiated on the higher terrain of eastern New Mexico ahead of the front. At 01 UTC, NOAA/NWS Storm Prediction Center mesoanalysis indicated 100 mb mixed-layer CAPE values of 1000 J/kg at the

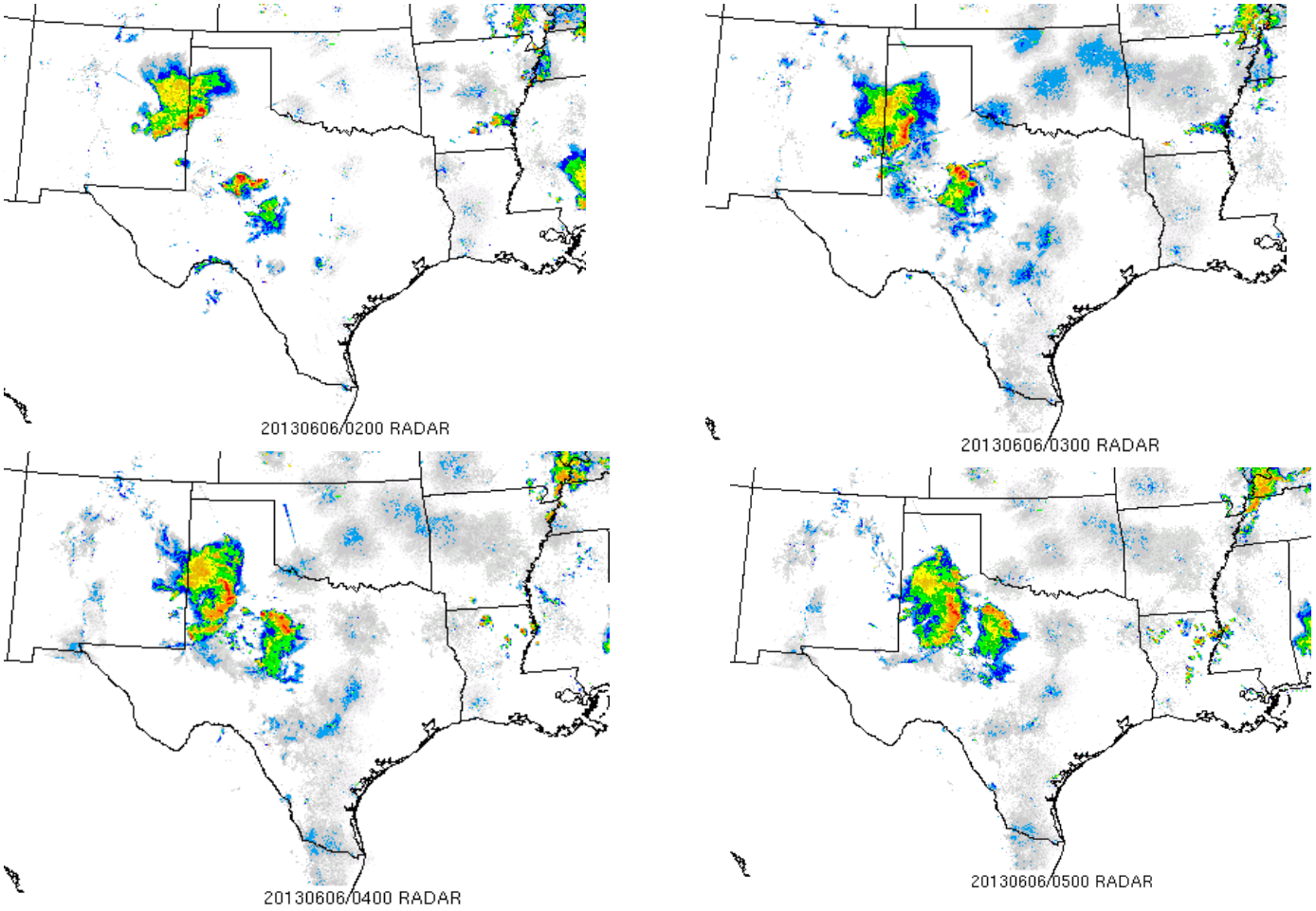

Fig. 1. Regional WSR-88D radar mosiacs between 02 and 05 UTC from NOAA/NWS/SPC (Progressing left to right through each row with time) showing storm evolution from the New Mexico border through West Texas.

New Mexico border to in excess of 3000 J/kg off the caprock to the east of Lubbock. At that time, the cold front remained just north of Lubbock, and extended to the west-northwest into New Mexico. By 02 UTC, the thunderstorms that initiated in New Mexico had congealed into a forward-propagating squall line with trailing stratiform region, and were crossing the New Mexico border, propagating into the higher-CAPE air and paralleling the cold front. Regional WSR-88D radar mosaics from NOAA/NWS/SPC (Figure 1) show that the storm was an asymmetric mesoscale convective system. The primary stratiform rain region was displaced well to the northwest [Parker:2000].

B. Local field observaions

Two TTU Ka-band radars [Weiss et al., 2009] and a set of StickNet [Schroeder and Weiss, 2008] surface instrumentation platforms were deployed by 0150 UTC in the vicinity of Pep, TX and began scanning shortly thereafter. Gunter and Schroeder [2013] summarize the deployment of these assets for the purpose of assessing the turbulent kinematic structure and vertical wind profile of severe wind events near the earth's surface. Early scans looked toward the approaching squall line, and observed the full depth of the troposphere before switching to a near-surface-focused scan strategy. After the conclusion of near-surface scans, an hour of continuous, full-troposphere RHI data was collected from 0300- 0410 UTC from a single radar looking due east toward the receding squall line. A new vertical slice was collected every 10 s at 0.33 deg beamwidth and ~10 m gate spacing out to 20 km range.

The West Texas Lightning Mapping Array provided lightning observations for this study. It is a recent version of the New Mexico Tech LMA system that has been operating continuously with nine stations since February 2012; a tenth station was added in May 2012. The WTLMA's stations are distributed in and around Lubbock County with a spacing of about 15 km. It operates at VHF channel 3 (60-66 MHz). Nine stations were active on 5-6 June 2013.

For this study, the flash plan-projection area was calculated by finding the area of the convex hull A_h of all VHF source points that comprise the flash. Flashes were sorted using the McCaul et al [2009] flash algorithm with grouping thresholds of 3 km and 0.15 s.

III. FLASH DATA ON 6 JUNE 2013

Fig. 2a-d shows the time series of flashes between 00 and 07 UTC for the entire squall line. There was a minimum in mean flash size between 0230 and 0430 UTC, which corresponded to the time when leading edge of the storm was within about 75 km of the WTLMA. The impact on the total energy was apparent, with the highest flash rates corresponding to a relative minimum in total energy. Note also that the flash size distribution was skewed.

The relative minimum in storm total flash energy corresponded to the smallest average flash sizes and was coincident with the time of the damaging winds near Lubbock — though severe weather was reported well before and after that time. The data showed that shifts in the average flash size could counteract an increase in flash rates, and in this case produced a relative minimum in electrical energy at the time of the greatest flash rate. To the extent this signal was meteorological, one might hypothesize that the storm's turbulent production increased at this time, thereby reducing the size of the charge pockets. Such thinking adds additional nuance to characterization of total lightning datasets: consideration of total energy allows for inference about trends in the fluid character of the thunderstorm region, beyond bulk mixed-phase updraft/downdraft trends [Williams et al. 1999].

Another view of the time trends, this time restricted to the cylinder directly above the LMA (range of 25 km, Fig. 2e-h) shows the influence on energy of a shift to larger flash sizes after 0400 UTC. While flash rates appear nearly negligible relative to the peak, the total energy remains an order of magnitude larger relative to the peak. The first flashes within range were of the small variety within the convective line, and then as the storm moved away and flash rates dropped, the influence of larger flashes in the trailing convection and transition zone of the mesoscale convective system were responsible in a shift in the average flash size to in excess of 15 km. These observations are consistent with the prediction of Bruning and MacGorman [2013] that turbulent convective regions are associated with the smallest flashes, and that infrequent but large flashes can be significant contributors to electrical energy.

Because the LMA produces more sources per flash at close range to the network, it is important to check whether network proximity is influencing the average flash size, leading to a low bias in size due to range effects that are independent of thunderstorm processes. At least two following non-meteorological factors are relevant. With range, a quadratic increase in range location errors and a linear increase in azimuth location errors [Thomas et al. 2004] and more low-power sources detected near the network, leading to more flashes that can meet the minimum-points-per-flash threshold at short ranges.

In order to understand the errors in flash area with range, we performed a monte carlo analysis of flash area errors. The model used circular flashes of radius R between 100 m and 100 km, at ranges to 300 km. The formulae from Thomas et al. (2004) for root-mean-square location errors in the range and azimuthal directions were used to generate Gaussian, zero-mean distributions of range and azimuthal position errors. The errors were used to perturb the original radius in the azimuthal and range directions, which produced an elliptical flash for small flash sizes and at ranges beyond 100 km. For a flash length scale l defined as the square root of the area, the analysis shows that, to 200 km range, the flash areas show less than 2% error for $l > 1.0$ km. The lack of sensitivity for flash sizes greater than 1 km is consistent with that derived from an analysis of sensitivity to flash sorting parameters in Bruning and MacGorman [2013].

A comparison of flash size statistics at close and far ranges tested whether the LMA was capable of resolving small flashes that might not produce sufficient numbers of powerful sources to be detected at long range. Weiss et al. (this conference) are also examining these issues, and they merit further study beyond what we present here. We compared the time series of average flash size in a ring from 75-100 km and from 0 to 75

km (Fig. 3). While fewer flashes were seen at longer range, there were times where the average flash size was at or below 5 km at each range interval. Futhermore, the trends in average flash size were the same at each range interval where there were at least enough flashes to produce a stable average, suggesting that the variation in flash size was at least in part meteorological.

IV. Radar Data on 6 June 2013

The TTU-Ka band radars collected equivalent radar reflectivity factor, doppler velocity, and spectrum width moments on 6 June 2013. Here, we present unfolded radial velocities. Fig. 4a-c shows sample data from 0224:46 UTC, looking toward the convective line. A highly turbulent updraft plume was observed at mid- to upper-levels, forced upward by an advancing gust front, whose nose was seen near the surface. Fig. 4d-f shows data from 0309:46 UTC, taken from the transition zone of the MCS, looking toward the receding convective line. The descending rear inflow jet was seen at low-levels, while front-to-rear flow was evident at upper levels.

Regions of turbulent and smooth flow are apparent in Fig. 4. Attenuation is significant at Ka band, but returns remain sufficiently coherent in velocity to 15-20 km range outside of the most significant precipitation cores. The resolute radar moments combined with RHI scans every 10 s along a single azimuth show scan-to-scan consistency in small-scale details of the velocity pattern. Gross regions of overturning, shear, wave motion, and even apparent updraft/downdraft motions were identified by eye while watching loops of the data. The measured radar moments show consistency with one another. Regions of greater texture (assessed visually) in the velocity data correspond to regions of enhanced spectrum width, suggesting that a three-method approach of aligning estimates from spectrum width, spatial statistics, and synthesized speed and direction along intersecting RHIs would be feasible for further quantitative work.

Furthermore, these data provide preliminary confirmation of this simple statement: more-turbulent regions with greater variance in radial velocity and larger spectrum width correspond to smaller flashes. All LMA sources within the 15 degrees azimuth angle of the RHI plane were plotted. Each source was colored according to the area of the flash to which the source belonged. Note the tiny, blue-colored VHF sources in the region of large spectrum width at 14 km range in Fig. 4a-c, and larger orange-colored flashes outside this region. Fig. 4d-f shows another important aspect of the data: there is usually some spread in flash sizes even within regions of larger spectrum width. That suggests that turbulent regions are a necessary but not sufficient condition for small flashes.

V. Concluding Remarks And Future Work

This study of a severe squall line further demonstrated the relationships between flash size and the texture of a thunderstorm's flow on the sub-cellular and whole-storm scale, as suggested by Bruning and MacGorman [2013]. The analysis showed that our proposed method of calculating flash energy provides additional information about the electrical activity that cannot be seen in flash rate alone. Some uncertainties remain about how the LMA's might distort the flash size distribution on the small end.

Our preliminary, qualitative comparison of Doppler radar-inferred kinematic texture will be expanded over the coming years as we conduct a focused observing campaign during the summers of 2015 and 2016. Observations of more storms across a range of storm modes will allow us to quantitatively compare flash size statistics to turbulence estimates derived from the spatiotemporal texture of radial velocities, spectrum width estimates, and dual-doppler wind profiles along intersecting vertical scans. In doing so, we expect to further establish the utility of the flash size and energy spectrum and explain its relationship to thunderstorm kinematic and dynamic morphology.

Acknowledgment

We thank Jonathan Hart for additional processing of the WTLMA data, and Brian Hirth for access to the data archive and details of the radar deployment. Numerous additional Texas Tech graduate students particpated in data collection on 6 June 2013, and we are grateful for their assistance in a successful mission.

References

Barthe, C. and M. C. Barth, 2008: Evaluation of a new lightning-produced NOx parameterization for cloud resolving models and its associated uncertainties. Atmos. Chem. Phys., 8, 4691–4710.

Bruning, E. C. and D. R. MacGorman (2013), Theory and observations of controls on lightning flash size spectra. J. Atmos. Sci., 70 (12), 4012–4029, doi:10.1175/JAS-D-12-0289.1.

Gunter, W. S. and J. L. Schroeder, 2013: High-resolution full-scale measurements of thunderstorm outflow winds. Proc. 12th Americas Conf. Wind Engineering, Seattle, WA, Paper 33.3.

McCaul, E. W., S. J. Goodman, K. M. La- Casse, and D. J. Cecil, 2009: Forecasting lightning threat using cloud-resolving model simulations. Weather and Forecasting, 24 (3), 709–729, doi:10.1175/2008WAF2222152.1.

Parker, M. D. and R. H. Johnson (2000): Organizational modes of midlatitude mesoscale convective systems. Monthly Weather Review, 128 (10), 3413–3436, doi:10.1175/1520-0493(2001)129<3413:OMOMMC>2.0.CO;2.

Schroeder, J. L. and C. C. Weiss (2008), Integrating research and education through measurement and analysis. Bulletin of the American Meteorological Society, 89 (6), 793–798, doi:10.1175/2008BAMS2287.1.

Schultz, C. J., W. A. Petersen, and L. D. Carey (2009):, Preliminary development and evaluation of lightning jump algorithms for the real-time detection of severe weather. J. Appl. Meteor. Climatol., 48, 2543–2563.

Thomas, R. J., P. R. Krehbiel, W. Rison, S. J. Hunyady, W. P. Winn, T. Hamlin, and J. Harlin (2004), Accuracy of the lightning mapping array. J. Geophys. Res., 109 (D14207).

Weiss, C. C., J. L. Schroeder, J. Guynes, P. S. Skinner, and J. Beck (2009), The TTUKa mobile Doppler radar: Coordinated radar and in situ measurements of supercell thunderstorms during Project VORTEX2. Preprints, 34th Conference on Radar Meteorology, Williamsburg, VA, USA, American Meteorological Society, paper 11B.2.

Williams, E. R., et al., 1999: The behavior of total lightning activity in severe florida thunderstorms. Atmos. Res., 51, 245–265.

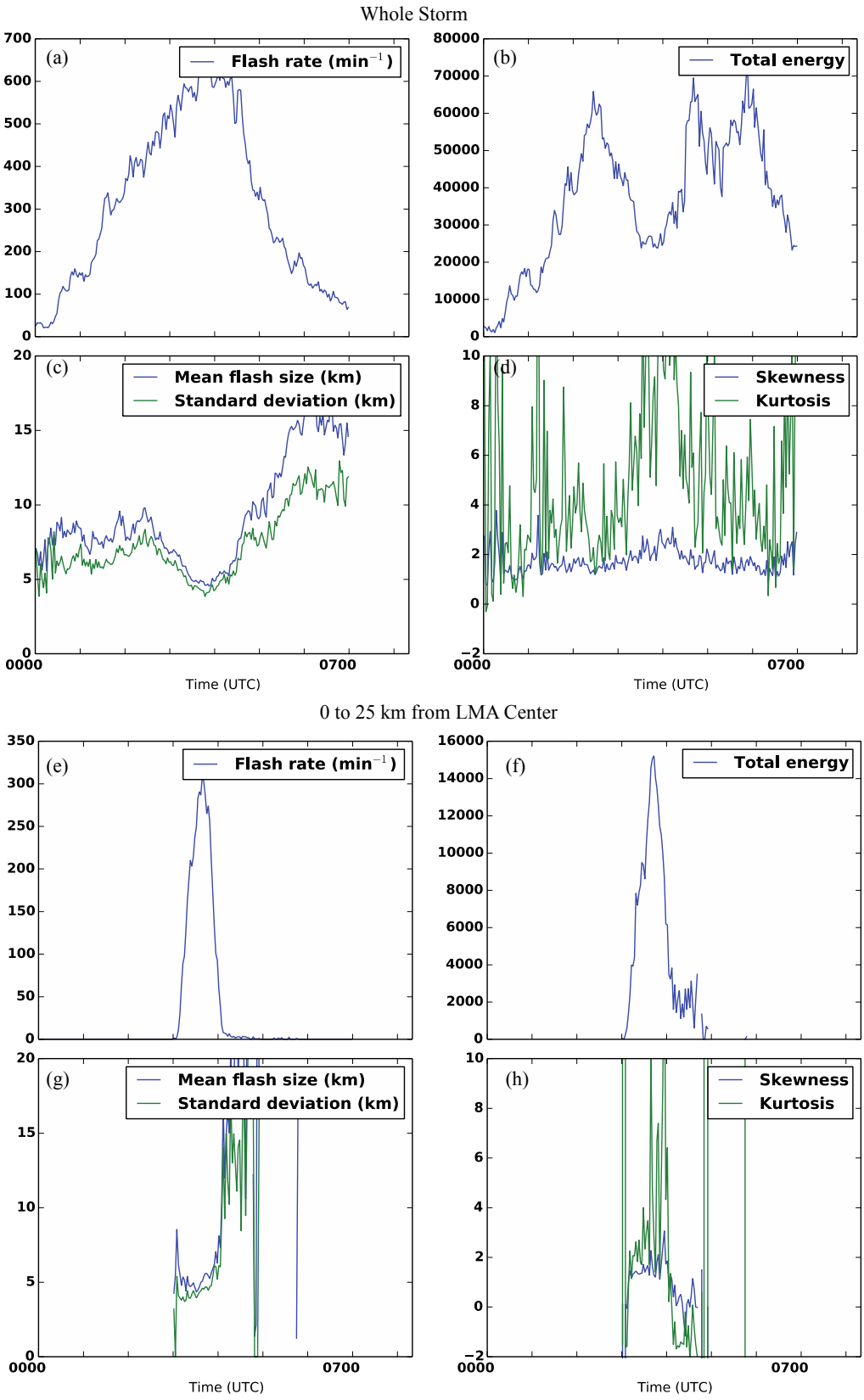

Fig. 2. Time series of flash statistics for 6 June 2013 between 00 and 07 UTC for (a–d) the entire storm and (e–h) only those flashes within 25 km of the center of the LMA. (a,e) Flash rate in flashes per minute. (b,f) Total flash energy in arbitrary units. (c,g) Average flash size and standard deviation in kilometers. (d,h) Skewness and kurtosis of the flash size distribution, where an unskewed distribution would have zero skewness.

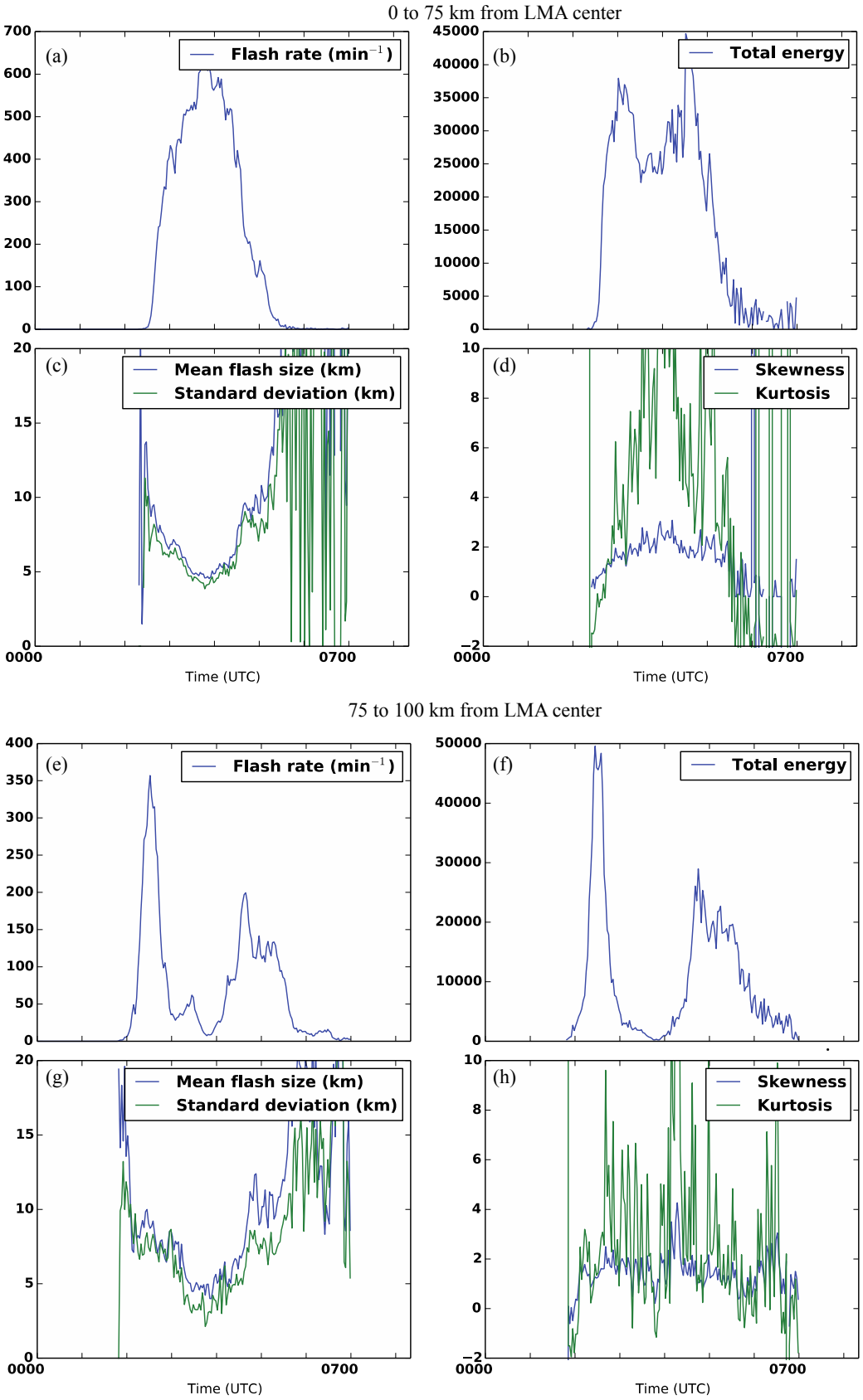

Fig. 3. Time series of flash statistics for 6 June 2013 between 00 and 07 UTC for (a–d) flashes within 75 km of the LMA center and (e–h) between 75 and 100 km. (a,e) Flash rate in flashes per minute. (b,f) Total flash energy in arbitrary units. (c,g) Average flash size and standard deviation in kilometers. (d,h) Skewness and kurtosis of the flash size distribution, where an unskewed distribution would have zero skewness.

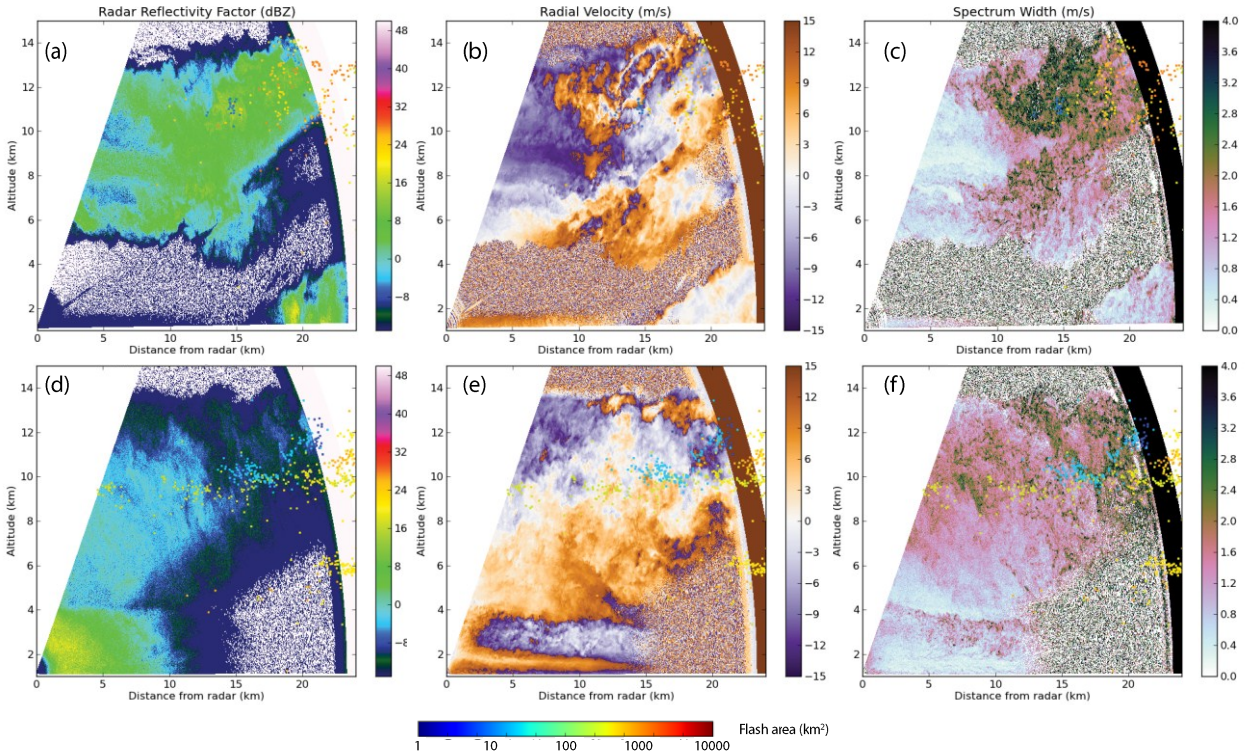

Fig. 4. Radar reflectivity factor, radial velocity (folds across the Nyquist velocity are present), and spectrum width from TTU-Ka1 on 6 June 2013 near Pep, Texas. LMA source points are overlaid and color-coded by flash horizontal area, with larger flashes in hot colors. Points not near the radar scan are not shown. (a--c) 0224:46-56 UTC, looking northwest toward the storm. (d--f) 0309:46-56 UTC, looking to the east toward the convective line. Reflectivity values are subject to strong attenuation, which is complete at about 8 km altitude and 20 km range in (a--c) and in the lower-right corner of (d--f)